



## ACCEPTED MANUSCRIPT

This is an early electronic version of an as-received manuscript that has been accepted for publication in the Journal of the Serbian Chemical Society but has not yet been subjected to the editing process and publishing procedure applied by the JSCS Editorial Office.

Please cite this article as S. Rengarajan, R. Muhammed, D. Vijayan, and M. Abrar, *J. Serb. Chem. Soc.* (2024) <https://doi.org/10.2298/JSC240224053R>

This “raw” version of the manuscript is being provided to the authors and readers for their technical service. It must be stressed that the manuscript still has to be subjected to copyediting, typesetting, English grammar and syntax corrections, professional editing and authors’ review of the galley proof before it is published in its final form. Please note that during these publishing processes, many errors may emerge which could affect the final content of the manuscript and all legal disclaimers applied according to the policies of the Journal.





*J. Serb. Chem. Soc.* **00(0)** 1-14 (2024)  
JSCS-12823

## Enhancing longevity and performance: the effects of ZrO<sub>2</sub> and TaC coatings on pistons in internal combustion engines

SATHISH RENGARAJAN<sup>1</sup>, RAMEEZA MUHAMMED<sup>1\*†</sup>, D. VIJAYAN<sup>2</sup>, AND  
MUHAMMED ABRAR<sup>3</sup>

<sup>1</sup>Department of Mechanical Engineering, St. Joseph's College of Engineering OMR, Chennai, Tamil Nadu, India, <sup>2</sup>Department of Mechanical Engineering, SCSVMV University, Enathur, Kanchipuram, Tamil Nadu, India, and <sup>3</sup>Department of Mechanical Engineering, St. Joseph's Institute of Technology, OMR, Chennai, Tamil Nadu, India.

(Received 24 February; revised 8 April; accepted 21 May 2024)

**Abstract:** Coating of pistons with ZrO<sub>2</sub> and TaC improves their longevity and performance in internal combustion engines by enhancing resistance to wear, heat, and corrosion. In this study plasma spray coating is performed on crown of the piston with the combination of the percentage composition namely, 95 % ZrO<sub>2</sub> + 5 % TaC, 98 % ZrO<sub>2</sub> + 2 % TaC and 100% ZrO<sub>2</sub>. Among the three 95% ZrO<sub>2</sub> + 5 % TaC composition shows better results. The increase in ZrO<sub>2</sub> content leads to the formation of a more integrated scale with fewer pores. Higher concentrations of ZrO<sub>2</sub> in the coatings lead to increased interaction with discharge sparks and instability of the process. At elevated temperatures, a two-phase material of cubic zirconium dioxide and hexagonal corundum was formed. The bonding strength of the coating is influenced by the addition of TaC and the power input during the spraying operation. The microstructure of ZrO<sub>2</sub> and TaC coatings on aluminium alloy is characterized by granular structure, tightly packed pores, and partially melted ZrO<sub>2</sub> particles. The coating had a uniform structure with columnar and cluster-like elements, influenced by ZrO<sub>2</sub> concentration.

**Keywords:** plasma spray; bond strength; scanning electron microscope; nano-particles.

### INTRODUCTION

The surface characteristics of engineering materials are regarded as crucial in the design process to improve the durability and functionality of components.<sup>1,2</sup> Wear, corrosion, or fatigue mechanisms are the most common causes of damage to engineering parts, which often begins at the surface and occurs during usage.

\* Corresponding author. E-mail: [rama.5.rsj@gmail.com](mailto:rama.5.rsj@gmail.com)

† Research Scholar

<https://doi.org/10.2298/JSC240224053R>

The thermal spray coating process is very adaptable and widely recognized as an efficient and cost-effective technique for surface engineering. The most prevalent technique for producing heat barrier coatings in production is plasma spray coatings. Its external high flame temperature makes it an ideal approach for spraying ceramic materials. This technique entails the creation of a coating by propelling small particles that are either melted, semi-molten, or softened towards the surface of the component. When particles strike repeatedly, they mechanically interlock with the surface they are deposited on, forming platelets called splats. These splats build up many layers, resulting in a coating with a certain thickness. The application of  $\text{ZrO}_2$  and TaC coatings on pistons is revolutionizing the automotive sector due to their remarkable durability and performance. These cutting-edge coatings, which are composed of tantalum carbide (TaC) and zirconium cobalt alloy ( $\text{ZrO}_2$ ), have great advantages that extend the life and efficiency of pistons in internal combustion engines.<sup>3,4</sup> Improving the resistance of pistons to wear, heat, and corrosion is the main goal of coating them with  $\text{ZrO}_2$  and TaC. These coatings have exceptional mechanical qualities, such as good temperature stability, low friction coefficient, and high hardness.<sup>3,5</sup> They can therefore tolerate the severe operating conditions found inside the engine, which include high temperatures, high pressures, and continuous friction.<sup>4-7</sup> Manufacturers can greatly increase the lifespan of pistons and lower the frequency of replacements and related maintenance expenses by using  $\text{ZrO}_2$  and TaC coatings. Furthermore, by lowering frictional losses and enhancing heat dissipation, these coatings help to improve fuel efficiency.<sup>6,8</sup> This results in decreased emissions, improved engine performance, and ultimately, a more ecologically friendly and sustainable driving experience. In recent times, there has been a substantial increase in the need for advanced materials exhibiting enhanced high-temperature characteristics. This surge in demand can be attributed to their pivotal role in diverse sectors including aerospace, energy, and automotive.<sup>7-10</sup> Materials used in high-temperature applications necessitate the preservation of their inherent properties and structural integrity across a range of temperatures. The criticality of high-temperature stability cannot be overstated when considering materials that are exposed to exceedingly elevated thermal conditions.<sup>9,11</sup> Thermal conductivity, an essential property, assumes a pivotal role in the processes of heat transfer and dissipation. The mechanical strength of materials holds significant importance, especially in high-temperature environments where maintaining structural integrity is crucial, alongside their thermal properties.<sup>10,12</sup> Hence, the investigation of superior mechanical, thermal, and thermomechanical properties is of paramount scientific significance. As the temperature rises, the physical and mechanical characteristics of materials experience alterations, resulting in a decline in material properties and diminished structural dependability.<sup>11,13</sup> Sivakumar and Kumar conducted a study to investigate the effects of Ytria

Stabilized Zirconia coating on the performance of diesel engines and the pollutants they produce.<sup>12,14</sup> A comparison was made between the impact of the thermal barrier coating (TBC) on the performance and emission metrics and the characteristic curves of the baseline engine. The material's notable characteristics, such as its high thermal expansion coefficient, low thermal conductivity, high Poisson's ratio, and stable phase structure at elevated temperatures, are easily noticeable.<sup>13-16</sup> The experiment improved thermal efficiency by 5 %, decreased heat loss to the cooling medium by 5 %, decreased HC emission by 35 %, decreased brake specific fuel consumption by 28.3 %, and raised thermal efficiency by 5 %. The aim of this research is to explore the impact of ZrO<sub>2</sub> and TaC coatings on a piston by altering their proportions. To the authors knowledge and from the above literature plenty of work has been carried on material performance coating on the piston to improve the efficiency like indicated power, fuel consumption, emission etc., only few researchers are focused in the evaluating of the Zirconium oxide and Tantalum coating. This study seeks to demonstrate the influence of varying coating percentages on the surface morphology and quality of the component. This report will present the surface features, microstructure as depicted in SEM images, and the mechanical attributes of the examined piston. The findings demonstrate that active polar oxygen-containing functional groups are introduced onto the PET surface as a result of plasma modification.<sup>34</sup> The coating provides exceptional resistance to exposure to abrasive chemicals, mechanical strength against extensive abrasion, and high hardness for the substrate.<sup>35</sup>

## EXPERIMENTAL PROCEDURE

### *Materials, methods, and experimentation*

The Tantalum carbide nano-powder was purchased by US Research Nano materials Inc., The ZrO<sub>2</sub> purchased sigma Aldrich. The chemical composition is shown in Fig. 1(a). The coating is performed on aluminium alloy which is used as a substrate shown in Fig. 1(b,c,d). The coating is done by plasma spray coating process using varying process parameters on Spraymet Surface Technologies Pvt. Ltd. Bangalore. Fig.1(e) shows the machine which consists of 3MB of plasma spray gun, Nozzle with GH type (Group hole) nozzle type, stand-off distance of maximum of 101mm with pressure of hydrogen of 3.5 bar and flow rate up to 450m/s. Samples were received and placed into a graphite crucible with a mixed powder composition of 95 %ZrO<sub>2</sub> + 5 % TaC, 98 %ZrO<sub>2</sub> + 2 % TaC, and 100 %ZrO<sub>2</sub>, then the coating was carried out on the samples using supersonic plasma spraying. The crucible was subsequently placed in a furnace and maintained at a temperature of 2000–2200°C for a duration of 2 hours. The TaC grains had a size ranging from 1–1.5 mm. The primary and carrier gas used was argon, while hydrogen served as the secondary gas. The samples were examined Field emission scanning electron microscope (FESEM) FEI make, Quanta 200F model. The chemical composition of the coated piston, which had different compositions, were analyzed using a FEGSEM and an attached energy-dispersive X-ray (EDX) spectrometer, the magnification varied from 10X-300,000X, with a resolution of 5nm. The X-ray diffraction (XRD) pattern of the ZrO<sub>2</sub>, TaC powder was obtained using a powder X-ray diffractometer done in SRM institute of Science

and Technology, Chennai having PAN analytical make with Benchtop Shimadzu model with CuK $\alpha$  radiation. The size of the crystallite was calculated by X-ray spectrum peaks using Scherrer's formula. To validate the coating, the samples are subjected to surface morphology and porosity measurement using Image analysis software with ASTM B487 standards (De-winter material plus version-2 with a magnification 50X-800X with 5 Megapixel camera at Metmech Analytical Engineers, Chennai).



Fig.1 (a) Chemical composition of Aluminum alloy, (b) 98% + 2 % TaC (c) 95 % ZrO<sub>2</sub> + 5 % TaC, (d) 100 % ZrO<sub>2</sub>, (e) Plasma spray machine (Spraymet Surface Technologies Pvt. Ltd.)

## RESULTS AND DISCUSSION

The Fig.2 shows the TaC and ZrO<sub>2</sub> powder XRD pattern reveals that presence of diffraction peaks in the pattern indicates a high degree of crystalline nature the diffraction angles TaC powder shows standard cubic structure with 2 theta value of 34.9260, 40.5480, 58.6870, 70.1470, 73.7650, 87.7400, TaC powder have pattern reflection of (h, k, l) of (02 0), (0 2 2) (1 3 1) (2 2 2) (0 4 0) which satisfy the JCPDS96-101-0655. Regarding the diffraction peaks of ZrO<sub>2</sub> shows monoclinic crystal system, they become more distinct and smaller, and their intensity noticeably increases. This indicates a significant improvement in the crystallinity of the ZrO<sub>2</sub> nanocrystals. The enhancement is due to the enlargement of particle size, which leads to an increase in the number of crystalline planes. 96-810-4265 JCPDS27.7920 (-1 1 1) 31.1190 (1 1 1) 34.8190 (200), 59.0520 (1 3 1)

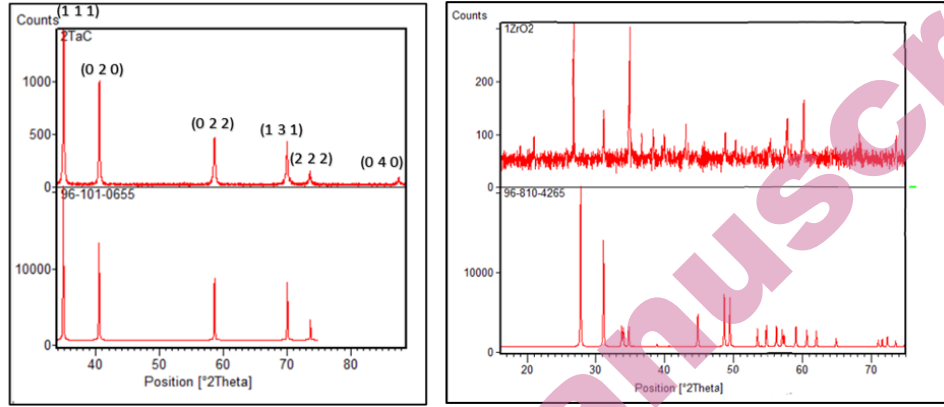


Fig. 2 XRD patterns for TaC and ZrO<sub>2</sub>

The EDS pattern signified the existence of Zr, C and, without any contamination from impurities shown in Fig. 3(a). In contrast, the interior layer, which has been partially oxidized, appears to be more compact and largely composed of ZrO<sub>2</sub> components. The micro-particle-like diameters of some ZrO<sub>2</sub> match XRD results, indicating amorphous compounds this agrees with the work.<sup>18-20</sup> The SEM image shows Fig. 3 (b) aggregation 100 nm of the average size having the appearance of the particles in shape of micro crystal with non-homogeneous particles sphere with interstitial spaces between the spheres. The Fig. 4 (a,b) shows the images acquired SEM, EDX of Tantalum powder which reveals the irregular or rise and fall surface.

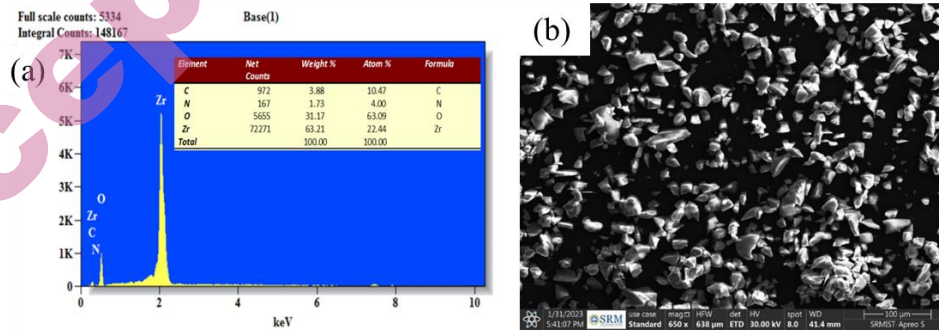


Fig. 3 (a) EDS (b) Powder SEM analysis for zirconium oxide



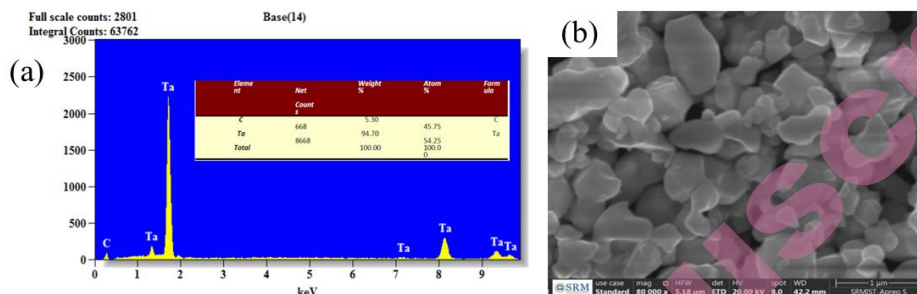


Fig. 4 (a) EDS (b) Powder SEM analysis for Tantalum carbide

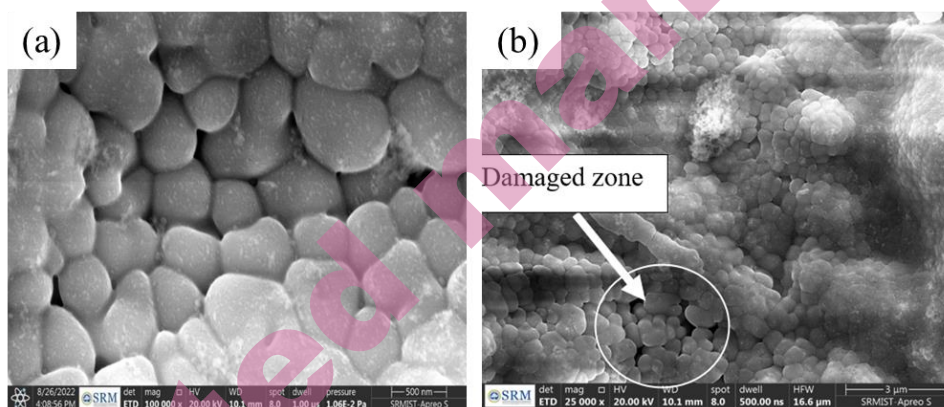
Fig. 5 (a) 100 % ZrO<sub>2</sub> coated aluminium alloy (b) Apparent gaps near the intersection (100 % ZrO<sub>2</sub> coated aluminium alloy)

Fig. 5 (a,b) reveals that the ZrO<sub>2</sub> coating on Aluminium alloy exhibits a granular structure with densely packed with pores. Inadequate heat conduction between the ZrO<sub>2</sub> particles during the deposition phase results in partial melting.<sup>15,21</sup> The amalgamation of partially and entirely liquefied ZrO<sub>2</sub> particles results in the formation of pores on the surface. When ZrO<sub>2</sub> is sprayed, it has a reaction with the gas molecules nearby, leading to a proper distribution of the coating on the substrate. The presence of oxide molecules in the air acts as a barrier, preventing the molten ZrO<sub>2</sub> particles from adhering to the substrate during the deposition process.<sup>16, 22</sup> Moreover, the intense stress encountered during the solidification of ZrO<sub>2</sub> leads to the development of micro-cracks inside its structure. A layer of ZrO<sub>2</sub> has been applied to the surface of the aluminum alloy, resulting in a visible white zone. The spherical shape of the spray-dried composite powder is evident. The utilization of nanoscale particles as starting materials enables the fabrication of nanostructured powders that possess a homogeneous distribution of ZrO<sub>2</sub>. The stability of the ceramic coatings is ensured by the plasma spraying process, which allows for optimal fluidity and homogeneous heating.<sup>17,23</sup> The



coatings exhibit predominantly tetragonal  $\text{ZrO}_2$  phases, indicating successful suppression of the change to the monoclinic phase.

The coating composed of 95 %  $\text{ZrO}_2$  and 5 % TaC has a columnar structure and lacks sensitive regions such as grain boundaries, dislocations, and second-phase precipitates. The columns have a width ranging from 30 to 60  $\mu\text{m}$ . The structure of the coating exhibits quasi-regular vertical fissures that span the whole surface. The high-magnification photos reveal that the structural parts of the coating primarily have a size ranging from 0.2 to 1  $\mu\text{m}$ , which aligns with the size of the particles that collide with the surface of the substrate. The higher density of the SPS coating is linked to a larger average particle size of material clusters in the suspension, ranging from 1 to 5  $\mu\text{m}$ . The absence of un-melted particles in the coating suggests that the plasma jet has generated enough thermal power. The coating often exhibits a size structure with splats ranging in thickness from 1 to 3  $\mu\text{m}$ . The surface morphology changed from a common pancake-shaped structure to a cluster-shaped structure, depending on the concentrations of  $\text{ZrO}_2$  and TaC. Similar observations were also reported by Jakubowicz, Sopata.<sup>20,24</sup>

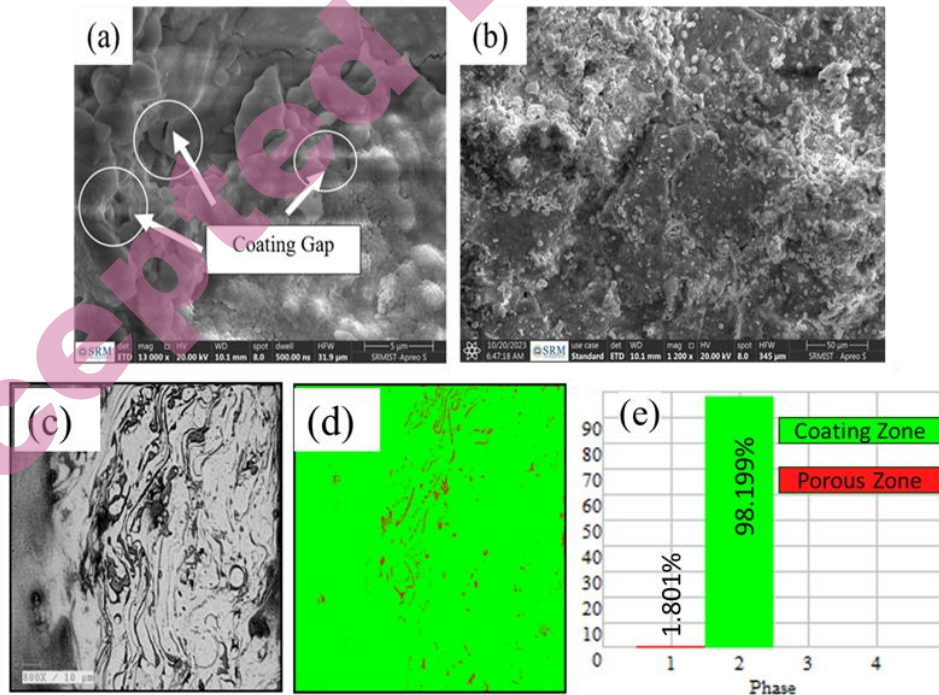


Fig. 6 (a) Morphology of the coated surface (b) Few pores on 95%  $\text{ZrO}_2$  +5% TaC Coating surface (c, d) Microstructure and Phase analysis (e) Porosity measurement

Furthermore, the interface layer of the 95 % ZrO<sub>2</sub> and 5 % TaC coatings does not show significant defects or pores due to the stability of the process shown in Fig.6(a,b). Fig.6(c,d) shows the microstructure of the intersection area which shows minimum pores. The porosity measurement shows that minimum pores area of 1.801% and the non porous area of 98.19% respectively shown in Fig.6(e). TaC particles were unable to react with aluminium, compromising the interfacial bonding strength.

The plasma spraying method causes these flaws when the surrounding gas interacts with the molten ZrO<sub>2</sub> droplets. Subsequently, when the droplets are deposited on the surface of the substrate, holes are formed due to inadequate overlap and quick solidification trapping internal gas.<sup>27</sup> The thickness of the coatings, as determined by cross-sectional analysis, increases simultaneously with ZrO<sub>2</sub> concentration. Beyond a concentration of 3 g/L of ZrO<sub>2</sub>, the inner layer suffered severe damage, leading to a halt in the increase of thickness. Nevertheless, up to this point, the trend of thickness increase becomes more prominent. This finding proves the ZrO<sub>2</sub> coating was adequately applied to the aluminum alloy. The presence of polyhedral or spherical grains, as well as unevenly formed grains, characterizes the densified microstructure. These granules are tightly bound together, providing a strong barrier that efficiently prevents oxygen from penetrating the piston material's surface.<sup>29</sup> Furthermore, the coating's structure contains a trace of mullite, which may be detected by its finest needle-shaped crystals. It should be noted that the powder rapidly melts and conducts a partial reaction with the oxygen present in the surrounding air during the spraying operation.

Microcracks, pores with dense structure are seen in the plasma-sprayed ZrO<sub>2</sub> coating, shown in Fig. 7(a,b). In the examination carried out by EDX shown in Fig. (7c), Zr was identified in the luminous sections of the TaC layer within the ZrO<sub>2</sub>-TaC coating applied on the aluminium alloy. In regards to the dynamic segregation theory for ZrO<sub>2</sub>, the reaction mechanism of ZrO<sub>2</sub> particles offers additional insight. It is theoretically possible for the reactive elements, even in their oxide form, to enhance oxidation resistance.<sup>18,25</sup> The participation of Zr in oxidation was observed in the study of ZrO<sub>2</sub> nanoparticles, ultimately being released from the ZrO<sub>2</sub> particles through reactions with Al.<sup>19,26</sup> Furthermore, the interfaces between the coatings and substrates are transparent and strongly adhered, and the resulting coatings are homogeneous, dense, and of sufficient quality

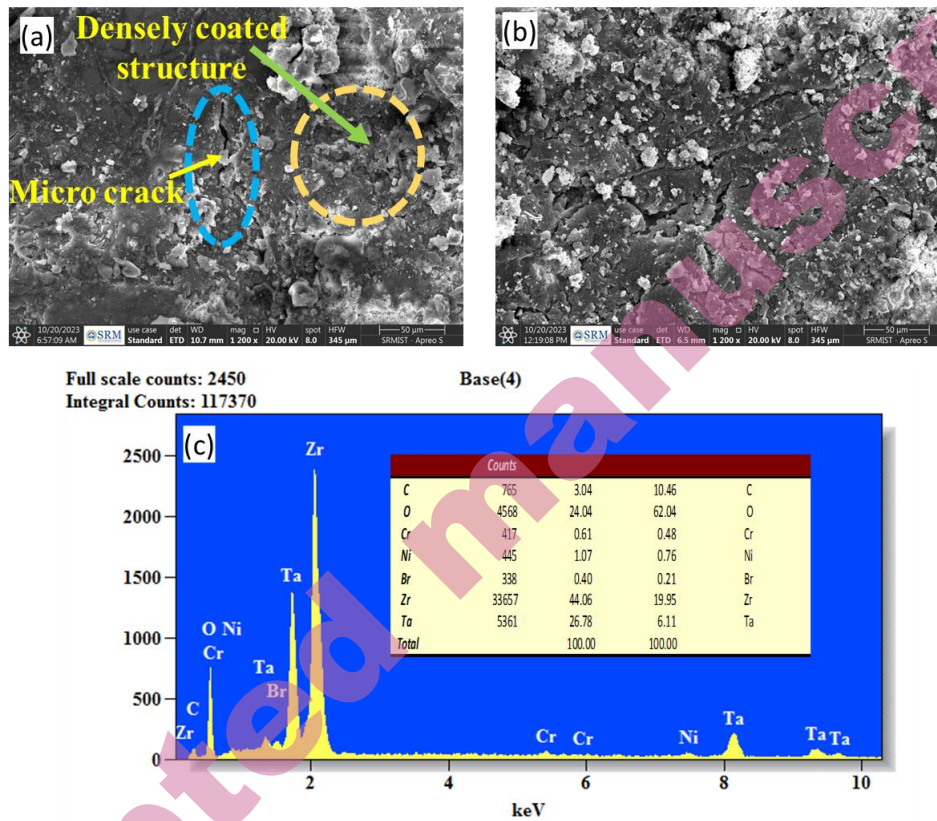


Fig. 7 (a) 95 %  $\text{ZrO}_2$  and 5 % TaC Zone of dense particle (b) Tiny pores on a coated surface (95 %  $\text{ZrO}_2$  and 5 % TaC), (c) EDX of the coated sample

This provides more evidence that the process is unstable at higher concentrations, more especially the nano particles concentration  $\text{ZrO}_2$  which is around 8 g/L. Damage is caused to the inner layer or interface when larger concentrations are present, such as when there is 98%  $\text{ZrO}_2$  and 2% TaC or when there is 100%  $\text{ZrO}_2$ .

The surface consisting of 98 %  $\text{ZrO}_2$  and 2 % TaC was entirely coated with a cluster-like formation. The presence of  $\text{ZrO}_2$  nanoparticles and localised plasma discharges contribute to the production of cluster-like formations. This phenomenon decreases the intensity of the discharges and causes instability.<sup>28</sup> With an increase in processing time, there is a corresponding increase in the size of the pancakes, which is a typical characteristic observed in plasma coating. Nevertheless, the impact of different  $\text{ZrO}_2$  concentrations on this rise was not as prominent. Furthermore, the morphology of the pancakes was altered as the concentration of  $\text{ZrO}_2$  increased, shifting from uniform spherical shapes to

irregular and fragmented shapes shown in Fig. (8a). The reason for this could be attributed to the elevated content of  $\text{ZrO}_2$ , which hampers the even dispersion of discharge channels. Regions that appear bright correspond to locations with a greater abundance of Zr, whereas regions that appear dark correspond to areas with a lesser abundance of Zr. The presence of brilliant patches around the discharge channel is observed for low concentrations of  $\text{ZrO}_2$ .<sup>29</sup> In addition, a multitude of minuscule pores appeared on the surface of the  $\text{ZrO}_2$  coating. These pores can be linked to the chemical reaction between Tac and the gaseous by products of  $\text{SiO(g)}$ ,  $\text{CO(g)}$ , and  $\text{H}_2\text{(g)}$ , Ni, N shown in Fig. (8b). Evidently, interlayer cracks, resulting from thermal mismatch, originated in the  $\text{ZrO}_2$  covering and separated the scale into two distinct sections. The damage occurs when a greater amount of  $\text{ZrO}_2$  species is transported through low-intensity discharge sparks, which do not induce interactions with the supplied species and thus harm the pre-existing inner layers. The porosity of this sample shows that maximum pore of 15.515% with coated area of 84.485% respectively shown in Fig. 8(c,d). The aforementioned trend is less conspicuous in coatings including 95 %  $\text{ZrO}_2$  with 5 % TaC, as well as those composed entirely of 100 %  $\text{ZrO}_2$ , when compared to the coating consisting of 98 %  $\text{ZrO}_2$  with 2 % TaC and its elements shown in Fig. (8e).

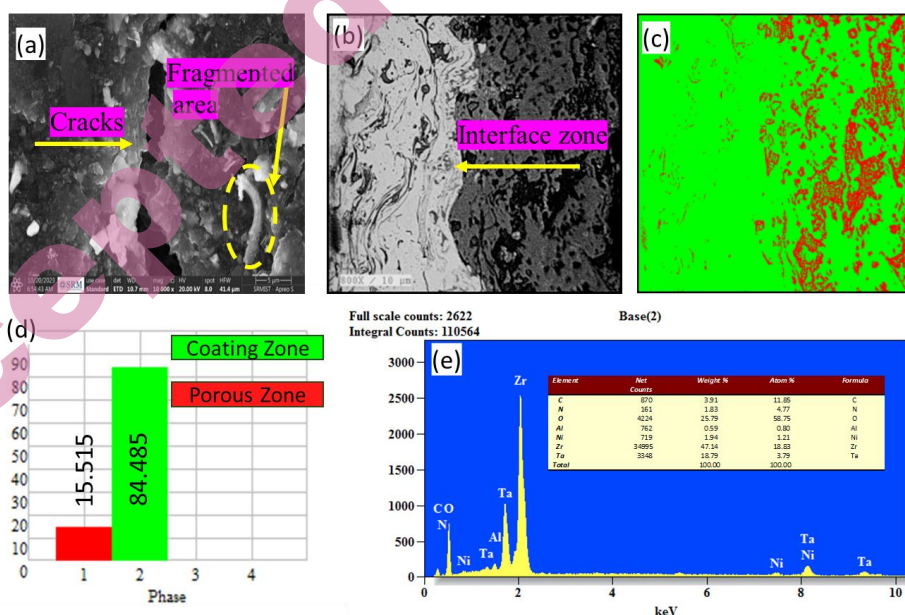


Fig. 8. (a) 98 %  $\text{ZrO}_2$  + 2 % TaC coating (b,c) Microstructure and Phase analysis (d) Porosity measurement (e) EDX analysis

Following a thorough analysis, it was identified that the spray-applied coating possesses a compact microstructure.<sup>30</sup> This microstructure is made up of totally

melted regions interspersed with a few particles that have remained un-melted. Surprisingly, a two-phase material is created within the coating when the temperature is elevated to 1400 °C.<sup>31</sup> This substance is made up of cubic zirconia dioxide, which has a white appearance, and hexagonal corundum, which has a dark gray appearance. Also the coating possesses occupied area of 84.485% and Porosity includes 15.515 %. Thus, it may be inferred that an increased concentration of ZrO<sub>2</sub> and an extended processing duration can lead to severe damage to the inner layers which is consistent with earlier reports.<sup>32,33</sup>

#### CONCLUSIONS

1. The microstructure of the zirconium dioxide (ZrO<sub>2</sub>) and titanium aluminium carbide (TaC) plays a crucial role in influencing the metallurgical and mechanical attributes of the surface coating. Oxide molecules in the air serve as a barrier, impeding the melted ZrO<sub>2</sub> particles from adhering to the substrate during deposition.
2. The appearance of the surface changed from a usual flat structure to a structure resembling clusters, with different amounts of ZrO<sub>2</sub> and TaC. Specifically, the surface with 98 % ZrO<sub>2</sub> and 2 % TaC was completely covered by the cluster-like structure.
3. Higher concentrations of ZrO<sub>2</sub> in the coatings lead to increased interaction with discharge sparks and instability of the process. Concentrations of 98 % ZrO<sub>2</sub> and 2 % TaC or 100 % ZrO<sub>2</sub> result in damage to the inner layer/interface. Higher concentrations and longer processing time can cause severe damage to the inner layers.
4. Plasma-sprayed ZrO<sub>2</sub> coatings exhibit microcracks and pores due to the interaction of gas with molten ZrO<sub>2</sub> droplets. The amount of thickness of the coatings is directly proportional to the concentration of ZrO<sub>2</sub> and the duration of the processing. Uneven layers and particle fusion are observed in the ZrO<sub>2</sub> coating, while the ZrO<sub>2</sub> coating has a relatively dense structure with cracks and tiny pores.
5. At elevated temperatures, a two-phase solid was made up of hexagonal corundum and cubic zirconia dioxide. It was made up of polyhedral or circular grains and a small amount of mullite.

*Acknowledgement:* The authors are very much thankful to St. Joseph's College of Engineering, OMR-Chennai.



## ИЗВОД

ПОВЕЋАЊЕ ДУГОВЕЧНОСТИ И ПЕРФОРМАНСИ: ЕФЕКТИ ZrO<sub>2</sub> И TaC ПРЕМАЗА НА КЛИПОВЕ У МОТОРИМА СА УНУТРАШЊИМ САГОРЕВАЊЕМSATHISH RENGARAJAN<sup>1</sup>, RAMEEZA MUHAMMED<sup>1†</sup>, D. VIJAYAN<sup>2</sup>, MUHAMMED ABRAR<sup>3</sup>

<sup>1</sup>Department of Mechanical Engineering, St. Joseph's College of Engineering OMR, Chennai, Tamil Nadu, India, <sup>2</sup>Department of Mechanical Engineering, SCSVMV University, Enathur, Kanchipuram, Tamil Nadu, India, and <sup>3</sup>Department of Mechanical Engineering, St. Joseph's Institute of Technology, OMR, Chennai, Tamil Nadu, India.

Облагање клипова са ZrO<sub>2</sub> и TaC побољшава њихову дуговечност и перформансе у моторима са унутрашњим сагоревањем повећавајући отпорност на хабање, топлоту и корозију. У овом истраживању вршило се наношење плазма спреја на круну клипа комбинацијом процентуалног састава и то 95% ZrO<sub>2</sub> + 5% TaC, 98% ZrO<sub>2</sub> + 2% TaC и 100% ZrO<sub>2</sub>. Најбоље резултате показао је састав 95% ZrO<sub>2</sub> + 5% TaC. Повећање садржаја ZrO<sub>2</sub> доводи до формирања интегрисаније скале са мање пора. Веће концентрације ZrO<sub>2</sub> у премазима доводе до повећане интеракције са варницама приликом процеса пражњења и доводе до нестабилности процеса. На повишеним температурама настаје двофазни материјал од кубног цирконијум диоксида и хексагоналног корунда. На снагу везивања премаза утиче додавање TaC, као и улазна снага током операције распршавања. Микроструктуру ZrO<sub>2</sub> и TaC превлака на легури алуминијума карактерише грануларна структура, чврсто збијене поре и делимично растопљене честице ZrO<sub>2</sub>. Превлака је имала уједначену структуру са стубастим и кластероликим елементима, под утицајем концентрације ZrO<sub>2</sub>.

(Примљено 24. јануара; ревидирано 8. априла; прихваћено 21. Маја 2024.)

## REFERENCES

1. P.L. Fauchais, J.V.R. Heberlein, M.I. Boulos, *Overview of Thermal Spray. In: Thermal Spray Fundamentals*. Springer, Boston MA, Springer, (2014) p. 17 ([https://doi.org/10.1007/978-0-387-68991-3\\_2](https://doi.org/10.1007/978-0-387-68991-3_2))
2. L. Pawlowski, *The Science and Engineering of Thermal Spray Coatings*, 2nd ed., Wiley, New York, 2008, ISBN 978-0-471-49049-4.
3. Y. Hu, Q. Dou, Q. Fu, X. Li, L. Zhou, J. Zhang, *Surf. Coat. Technol.* **435** (2022) 128243. (<https://doi.org/10.1016/j.surfcoat.2022.128243>)
4. Y. Zhang, J. Sun, L. Guo, X. Zhang, D. Cui, Q. Fu, *Corrosion Science* **205** (2022) 110423 (<https://doi.org/10.1016/j.corsci.2022.110423>)
5. Z. Fu, X. Li, Y. Ren, M. Zhang, X. Geng, Q. Zhu, J.G. Li, X. Sun, *J. Eur. Ceram. Soc.* **39** (2019) 4996 (<https://doi.org/10.1016/j.jeurceramsoc.2019.07.011>)
6. Z. L. Mao, X. J. Yang, S. L. Zhu, Z. D. Cui, Z. Y. Li, Y. Q. Liang, *Mater. Express.* **5** (2015) 518 (<https://doi.org/10.1166/mex.2015.1267>)
7. G. Feng, H. Li, X. Yao, L. Chen, Y. Yu, H. Wang, and M. Chen, *Ceram. Int.* **47** (2021) 21721 (<https://doi.org/10.1016/j.ceramint.2021.04.187>)
8. N. B. Dahotre, S. J. S. Nayak, *Surf. Coat. Technol.* **194** 2005 58 (<https://doi.org/10.1016/j.surfcoat.2004.05.006>)
9. Z. Yao, Z. Song, H. Hao, Z. Yu, M. Cao, S. Zhang, M.T. Lanagan, H. Liu, *Adv. Mater.* **29** (2017) 1601727 (<https://doi.org/10.1002/adma.201601727>)



10. C. Suryanarayana, *Research*, **10** (2019) 4219812 (<https://doi.org/10.34133/2019/4219812>)
11. V. Gvozdetzkyi, B. Owens-Baird, S. Hong, and J.V. Zaikina, *Mater.* **12** (2018) 48 (<https://doi.org/10.3390/ma12010048>)
12. L. Wang, D. C. Li, J. S. Yang, F. Shao, X. H. Zhong, H. Y. Zhao, K. Yang, S. Y. Tao, Y. Wang, *J. Eur. Ceram. Soc.* **36** (2016) 1313 (<https://doi.org/10.1016/j.jeurceramsoc.2015.12.038>)
13. R. Darolia, *Int. Mater. Rev.* **58** (2013) 315 (<https://doi.org/10.1179/1743280413Y.0000000019>)
14. G. Sivakumar, S. S. Kumar, *Alex. Eng. J.* **53** (2014) 787 (<https://doi.org/10.1016/j.aej.2014.08.003>)
15. E. Vural, S. Ozel, B. Ozdalyan, *Optoe. Adv. Mat.* **8** (2014) 515 (<https://oam-rc.inoe.ro/articles/the-investigation-of-microstructure-and-mechanical-properties-of-oxide-powders-coated-on-engine-pistons-surface/fulltext>)
16. J. Liang, Z. Peng, R. Li, B. Wang, *Ceram. Int.* **49** (2023) 29133 (<https://doi.org/10.1016/j.ceramint.2023.06.192>)
17. L. K. Brar, G. Singla, O. P. Pandey, *RSC. Adv.* **5** (2015) 1406 (<https://doi.org/10.1039/C4RA12105H>)
18. R. Sukanya, S. Ramki, S. M. Chen, *Microchim. Acta* **187** (2020) 342 (<https://doi.org/10.1007/s00604-020-04314-7>)
19. D. Manoharan, A. Loganathan, V. Kurapati, V. J. Nesamony, *Ultrason. Sonochem.* **23** (2015) 174 (<https://doi.org/10.1016/j.ultsonch.2014.10.004>)
20. E. A. Abdel Wahab, K.S. Shaaban, R. Elsaman, E. S. Yousef, *Appl. Phys. A* **125** (2019) 869 (<https://doi.org/10.1007/s00339-019-3166-8>)
21. M. Kovaleva, I. Goncharov, V. Novikov, M. Yapryntsev, O. Vagina, V. Sirota, Y. Tyurin, O. Kolisnichenko, *Mater. Today: Proc.* **49** (2022) 1423 (<https://doi.org/10.1016/j.matpr.2021.07.132>)
22. I. Gulyaev, V. Kuzmin, E. Kornienko, S. Vashchenko, D. Sergachev, *Mater. Today: Proc.* **11** (2019) 430 (<https://doi.org/10.1016/j.matpr.2019.01.008>)
23. Z. U. Rehman, D. Choi, *J. Magnes. Alloys* **7** (2019) 555 (<https://doi.org/10.1016/j.jma.2019.10.001>)
24. J. Jakubowicz, M. Sopata, G. Adamek, P. Siwak, T. Kachlicki, *Adv. Mater. Sci. Eng.* **2018** (2018) 2085368 (<https://doi.org/10.1155/2018/2085368>)
25. B. A. Pint, *Oxid. Met.* **45** (1996) 1 (<https://doi.org/10.1007/BF01046818>)
26. X. Luo, X. Yang, Q. Huang, A. Shi, C. Fang, Y. Weng, *J. Therm. Spray Technol.* **30** (2021) 1582 (<https://doi.org/10.1007/s11666-021-01215-w>)
27. G. Shao, Q. Wang, X. Wu, C. Jiao, S. Cui, Y. Kong, J. Jiao, X. Shen, *Corros. Sci.* **126** (2017) 78 (<https://doi.org/10.1016/j.corsci.2017.06.017>)
28. Y. H. Cui, Z. C. Hu, Y. D. Ma, Y. Yang, C. C. Zhao, Y. T. Ran, P. Y. Gao, L. Wang, Y. C. Dong, D. R. Yan, *Surf. Coat. Technol.* **363** (2019) 112 (<https://doi.org/10.1016/j.surfcoat.2019.02.059>)
29. G. Shao, X. Wu, S. Cui, X. Shen, Y. Lu, Q. Zhang, Y. Kong, *J. Alloys Compd.* **690** (2017) 63 (<https://doi.org/10.1016/j.jallcom.2016.08.073>)
30. A. A. Ali, S. A. Shama, A. S. Amin, S. R. EL-Sayed, *Mater. Sci. Eng. B* **269** (2021) 115167 (<https://doi.org/10.1016/j.mseb.2021.115167>)
31. R. Vaßen, D.E. Mack, M. Tandler, Y. J. Sohn, D. Sebold, O. Guillon, *J. Am. Cer. Soc.* **104** (2021) 463-71 (<https://doi.org/10.1111/jace.17452>)

32. D. Wang, B. Yang, Z. Tian, L. Shen, Y. Huang, *Trans. China Weld.* **34** (2013) 10 (<http://hjxb.hwi.com.cn/hjxb/en/article/id/20130303>)
33. K. H. Kim, S. Hoon, J. H. Kim, K. W. Hong, J. Y. Park, *J. Nanosci. Nanotechnol.* **17** (2017) 8598 (<https://doi.org/10.1166/jnn.2017.15171>)
34. S. Samipour, H. Taghvaei, D. Mohebbi-Kalhari, M. R. Rahimpour, *Surf. Innov.* **8** (2019) 76 (<https://doi.org/10.1680/jsuin.19.00030>)
35. K. Zhang, Y. Zhu, Z. Chen, Z. Zhang, Y. Gao, *Surf. Innov.* **40** (2022) 1 (<https://doi.org/10.1680/jsuin.22.01049>).